

LangFlash: Feed-forward 3D Language Gaussian Splatting from Sparse Unposed Images

Yilong Liu^{1,3} Wanhua Li^{1,2,*} Chen Zhu-Tian⁴ Hanspeter Pfister¹
¹Harvard University ²Nanyang Technological University
³Tsinghua University ⁴University of Minnesota - Twin Cities

liuyilon22@mails.tsinghua.edu.cn, wanhua.li@ntu.edu.sg, ztchen@umn.edu, pfister@seas.harvard.edu

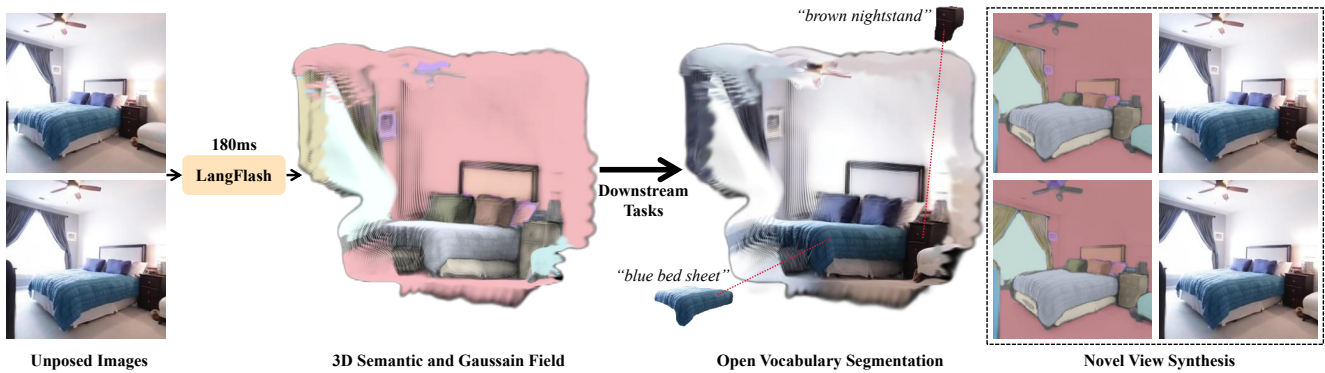


Figure 1. LangFlash reconstructs 3D semantic Gaussian fields directly from sparse unposed multi-view images in a single forward pass. Given unposed input images, LangFlash predicts geometry and semantics within 180 ms, producing a unified 3D Semantic and Gaussian Field that supports multiple downstream tasks, including open-vocabulary 3D segmentation and novel view synthesis.

Abstract

We present *LangFlash*, a feed-forward framework for 3D Language Gaussian Splatting that reconstructs 3D scenes parameterized by Gaussian primitives enriched with language-aligned semantic features from sparse unposed multi-view images. Unlike optimization-based 3D methods, *LangFlash* directly predicts the geometry and semantics in a single forward pass, enabling low-latency 3D reconstruction and language-consistent scene understanding. To support large-scale training, we enriched the *RealEstate10k* dataset with coherent and dense semantic information for 3D semantic supervision. Furthermore, we propose a sparse semantic encoding scheme that combines a global semantic dictionary with locally varying per-primitive weights, preserving high-level linguistic information, while reducing representation complexity. Experimental results show that *LangFlash* achieves superior novel view synthesis and semantic consistency compared with previous methods. This study establishes a new paradigm for pose-free, language-grounded 3D scene

reconstruction, advancing generalizable 3D vision and multimodal scene understanding. Code is available at <https://liylo.github.io/langflash.github.io/>.

1. Introduction

3D scene reconstruction [8, 38] is a fundamental problem in computer vision. Recent advances have significantly improved the realism of applications in embodied AI and robotics, while also enabling novel view synthesis to enhance environmental perception and understanding [7, 58].

Despite progress on both optimization-based [13, 31] and feed-forward [2, 4, 11, 37, 52] methods, current approaches remain restricted to geometry and appearance, without incorporating semantics. However, semantics are essential for high-level reasoning and decision-making because they provide structured representations of the environment. Therefore, a unified framework that jointly reconstructs the geometry, appearance, and semantics in 3D is desirable. Moreover, existing semantic models [19, 28, 30, 48, 51] typically operate on 2D observations and cannot embed semantics into 3D representations, limiting novel view

* Corresponding author

inference and comprehensive scene understanding.

Earlier attempts have incorporated semantics into NeRF [14, 15, 25, 55], but the inefficiency of implicit representations results in poor performance under sparse-view inputs. More recent efforts have extended 3DGS to semantic fields [22, 23, 33, 46, 50, 56], yet these still rely on per-scene optimization and lack cross-scene generalization. Other attempts [3, 10, 21] directly project fine-grained pixel-aligned language features onto Gaussian points predicted by feed-forward models, allowing the reconstruction of the semantic field in a relatively faster manner. However, constructing such fine-grained features requires time-consuming segmentation and tracking models as preprocessing steps, making them unsuitable for real-time reconstruction.

The latest LSM framework [9] moves toward the feed-forward estimation of geometry, appearance, and semantics, offering notable efficiency over optimization-based approaches. However, its strategy of directly downsampling and regressing high-dimensional language features fundamentally limits the quality of semantic reconstruction. High-dimensional embeddings contain fine-grained semantic cues, and aggressive downsampling inevitably discards the key semantic information and contextual relations required for accurate 3D grounding. The resulting features also exhibit cross-view inconsistencies, and regressing these noisy, high-dimensional vectors imposes a heavy training burden, which slows convergence and leads to unstable semantic predictions. Furthermore, storing and rendering such high-dimensional features during inference is computationally expensive. These limitations underscore the need for a more compact, structured, and semantically aligned framework that preserves linguistic meaning while remaining efficient for feed-forward 3D reconstruction.

To address these limitations, we propose LangFlash, a novel generalizable framework that synthesizes a unified 3D representation from arbitrary sparse images for both high-fidelity rendering and dense open-vocabulary semantic understanding. The proposed model is powered by a large dataset, RealEstate10k (RE10k) [57] (over 10M frames), with semantic information that we have labeled. By leveraging the *Semantic Grouping* and *Language Feature Aggregation* modules, our approach effectively integrates information from multi-view RGB images and semantic maps, yielding globally consistent representations. LangFlash predicts unified 3D Gaussian primitives that are enriched with open-vocabulary semantic features. These Gaussian representations can be seamlessly rendered with low latency to synthesize novel views, bypassing the need for per-scene optimization.

To balance the semantic expressiveness and computational efficiency in feature prediction, we introduced a sparse feature-encoding scheme. Specifically, we first construct a high-dimensional global dictionary from the input

image that captures a wide range of semantic information. Instead of directly predicting high-dimensional feature vectors, the model estimates only sparse weights corresponding to the entries in the global dictionary. This design significantly reduces the computational and storage overheads while preserving the expressive power of the semantic features.

Our contributions are summarized as follows.

- We enrich the RE10k [57] dataset with coherent semantic information, where every pixel in every frame of each video is associated with a high-quality, temporally consistent dimensional semantic feature.
- We introduce LangFlash, a novel feed-forward architecture that unifies 3D reconstruction and semantic understanding. Instead of directly regressing language features, it predicts a global semantic dictionary with locally varying, per-primitive weights.
- Experimental results show that our method not only achieves superior performance in both novel view synthesis and 3D open-vocabulary segmentation, but also delivers an inference speed of only 180 ms per scene.

2. Related Works

Feed-Forward Reconstruction. Classical methods such as NeRF [31] and 3D Gaussian Splatting [13] produce high-quality novel views by optimizing a scene-specific representation at test time, which is computationally expensive and unsuitable for real-time use. In contrast, feed-forward approaches learn priors from large datasets and perform one-shot or few-shot inference without per-scene optimization; these methods directly predict 3D representations (e.g., point maps, point clouds, or Gaussian primitives) from sparse, possibly unposed images, enabling fast and generalizable reconstruction [2, 4, 11, 37, 52]. Recent studies have further eliminated the need for known camera poses by predicting the geometry and appearance in a canonical frame from uncalibrated inputs. In particular, transformer-based 3D reconstruction priors (e.g., DUS3R [41], MAST3R [18], and VGGT [40]) cast matching and reconstruction as 3D pointmap regression and enable pose-free or pose-agnostic reconstruction. Building on these geometric priors, Gaussian-based feed-forward methods such as Splatt3R [37] and other zero-/few-shot splatting approaches directly infer splat parameters from uncalibrated images for fast rendering [12, 42, 49]. Overall, feed-forward models demonstrate impressive inference speed and cross-scene generalization, making them attractive for embodied agents and interactive systems [2, 4].

Semantic-aware 3D Representations. Embedding semantics into 3D representations has been explored in both implicit (NeRF-based) and explicit (e.g., Gaussian splatting) families. Early implicit efforts extended NeRF to include semantic outputs supervised by 2D labels, enabling novel-

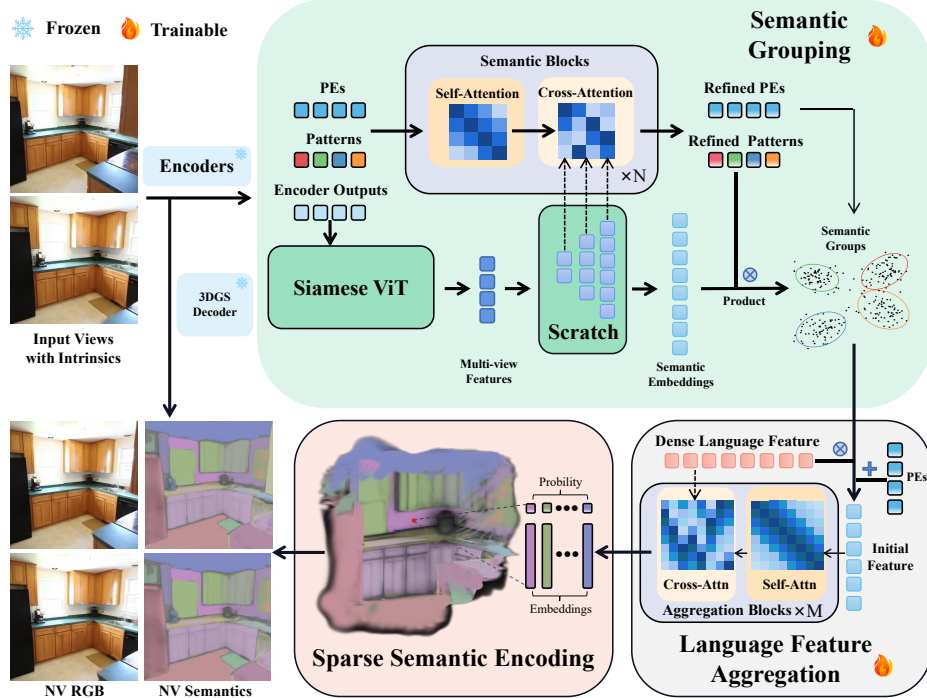


Figure 2. The overall architecture of LangFlash is illustrated as follows. Features extracted by the shared image encoders are first passed to a pretrained 3D Gaussian decoder to reconstruct scene geometry. In parallel, learnable positional embeddings, learnable patterns, and encoder outputs are processed by the semantic grouping module. The resulting groups, together with the refined positional embeddings, are then fed into the language feature aggregation stage, where coarse dense language features from a pretrained CLIP-like model are further refined to produce the final embeddings for each selected group. Outputs from all preceding modules are finally integrated to form the complete 3D semantic representation.

view semantic synthesis but inheriting the computational cost of per-scene optimization [14, 15, 25, 55]. Explicit 3D Gaussian approaches have recently been extended to include semantic components or to distill 2D semantic models into 3D primitives, enabling open-vocabulary or dense semantic 3D representations [33, 46, 50, 56]. However, many of these studies still rely on per-scene optimization. More recently, generalizable feed-forward models [9] jointly predict geometry, appearance, and semantics from unposed inputs in a single forward pass, moving the field toward pose-free, semantic-aware, and real-time 3D understanding. Our LangFlash follows this direction by operating in a pose-free, feed-forward framework built upon 3D Gaussian primitives while tightly integrating open-vocabulary semantic features into the representation to achieve a balance between efficiency and reconstruction accuracy.

3. Method

3.1. Feed-Forward Semantic Gaussian Splatting

Overview. Our model accepts unposed input images together with corresponding camera intrinsics and outputs an efficient semantic Gaussian field, which will be described

in 3.2. We first build on a pretrained NoPospalt [49] network and freeze it. The features from its encoder are then fed into a *Semantic Grouping* module to produce semantic groups. Subsequently, the semantic groups, together with language features extracted by a pretrained vision-language model [19], are processed by a *Language Feature Aggregation* module to obtain fine-grained features for each semantic group, which are then used to form the scene’s semantic Gaussian representation.

Semantic Grouping. The Semantic Grouping module takes the encoder’s multi-view outputs as input. We employ a Siamese ViT-based decoder to [43] produce multi-scale outputs for every view, and a scratch head refines each view’s multi-scale outputs [35] to produce multi-view, multi-scale dense semantic maps. We concatenate these refined outputs along the view dimension to form a scene-level, multi-scale dense feature field $F(\mathbf{x})$ defined at each spatial location, \mathbf{x} . Finally, we add 1D sinusoidal positional encodings [39] to the scene’s multi-scale outputs.

Following the DETR-like [1, 5, 20, 27, 53] designs, we maintain N learnable pattern vectors (queries) $\{q_n\}_{n=1}^N$ and positional embeddings $\{r_n\}_{n=1}^N$. We add positional em-

beddings to the queries in all subsequent layers. The processed queries undergo self-attention for refinement. Subsequently, cross-attention between the refined queries and dense features provides the queries with knowledge of the 3D structure of the scene. Each query eventually passes through an MLP head to predict its group existence probability $p_n(\mathbf{x})$ at spatial location \mathbf{x} in the scene. To obtain a compact and variable-length representation, we filter out inactive queries using the threshold $p_n(\mathbf{x}) > \tau_{\text{exist}}$, resulting in K valid semantic groups ($K \leq N$). For these surviving K groups, we apply a softmax operation across the group dimension to obtain normalized probability maps $w_k(\mathbf{x})$ for $k = 1, \dots, K$. For a Gaussian primitive i located at \mathbf{x}_i , this continuous probability directly yields its semantic weight $w_{ik} = w_k(\mathbf{x}_i)$, which will be explained in Section 3.2.

Language Feature Aggregation. We utilize a pretrained vision-language model [19] to extract a downsampled language feature map $L(\mathbf{x})$, which is bilinearly interpolated back to the input resolution.

Using the derived semantic weights, the initial feature for each valid group k is aggregated as

$$\mathbf{d}_k^{(0)} = \frac{\sum_{\mathbf{x}} w_k(\mathbf{x}) L(\mathbf{x})}{\sum_{\mathbf{x}} w_k(\mathbf{x}) + \epsilon}. \quad (1)$$

Subsequently, our aggregation block updates this initial group feature using multiple transformer blocks. Within each block, we conduct cross-attention between the group features and the language feature map $L(\mathbf{x})$ to obtain the final refined semantic dictionary atom, \mathbf{d}_k . From the Semantic Grouping and Language Feature Aggregation modules, we obtain the per-primitive weights w_i and the global dictionary $\mathcal{D} = \{\mathbf{d}_k\}_{k=1}^K$, providing sufficient elements to reconstruct the 3D semantic Gaussian field detailed in Section 3.2.

Semantic Grouping Loss. The predicted groups are matched to the ground-truth groups using Hungarian matching [1]. For matched groups, we apply a focal loss L_{focal} [24] and dice loss L_{dice} [32]. The unmatched groups are supervised using an existence loss L_{exist} [1].

We also apply dense supervision from a SAM [16] encoder output $S_{\text{SAM}}(\mathbf{x})$ using:

$$L_{\text{MSE}} = \|F(\mathbf{x}) - S_{\text{SAM}}(\mathbf{x})\|_2^2. \quad (2)$$

Total Semantic Grouping loss:

$$L_{\text{SG}} = \lambda_{\text{focal}} L_{\text{focal}} + \lambda_{\text{dice}} L_{\text{dice}} + \lambda_{\text{exist}} L_{\text{exist}} + \lambda_{\text{mse}} L_{\text{MSE}}. \quad (3)$$

Language Feature Aggregation Loss. For the Language Feature Aggregation (LFA) module, we supervise the refined feature with three objectives: consistency with the input feature, alignment to the ground-truth language feature,

and, when text labels are available, additional alignment to the text embedding. Moreover, if text labels exist, we modulate the GT alignment weight using the cosine similarity between the GT feature (its derivation will be discussed in 3.3, denoted as g_n^{gt}) and the text embedding (denoted as t_n), so that only positive-correlated pairs contribute.

The input consistency loss is defined as follows:

$$L_{\text{in}} = \frac{1}{N} \sum_{n=1}^N \left(1 - \cos(\mathbf{d}_n, \mathbf{d}_n^{(0)})\right). \quad (4)$$

The GT alignment loss is:

$$L_{\text{gt}} = \frac{1}{N} \sum_{n=1}^N p_n \left(1 - \cos(\mathbf{d}_n, g_n^{\text{gt}})\right), \quad (5)$$

where the adaptive weight p_n is defined as:

$$w_n = \begin{cases} \max\{0, \cos(g_n^{\text{gt}}, t_n)\}, & \text{if text label } t_n \text{ is available,} \\ 1, & \text{otherwise.} \end{cases} \quad (6)$$

When text labels are available, we further apply text alignment loss as follows:

$$L_{\text{text}} = \frac{1}{N} \sum_{n=1}^N \left(1 - \cos(\mathbf{d}_n, t_n)\right). \quad (7)$$

The total LFA loss combines all terms, where the text-related term is activated only when text labels are provided:

$$L_{\text{LFA}} = \lambda_{\text{in}} L_{\text{in}} + \lambda_{\text{gt}} L_{\text{gt}} + \mathbb{I}_{\{\text{text}\}} \lambda_{\text{text}} L_{\text{text}}. \quad (8)$$

Here, $\mathbb{I}_{\{\text{text}\}}$ is an indicator function that equals 1 when the text labels are available and 0 otherwise.

Training Schedule We first train the Semantic Grouping module using L_{SG} while freezing geometry. Then, we freeze them all and train the Language Feature Aggregation module using L_{LFA} . This schedule stabilizes the convergence and improves the consistency of the multiview.

3.2. Sparse Semantic Encoding

We represent the semantics of a scene using sparse encoding that combines a global semantic dictionary with locally varying per-primitive weights. As described in 3.1, given sparse input images, we first reconstruct the Gaussian field and predict the corresponding semantic groups. Next, we extract semantic features $\mathcal{F}(\mathbf{x})$ using a pretrained language feature extractor [19]. Based on these semantic groups, we then pool and refine the features to obtain the global semantic dictionary

$$\mathcal{D} = \{\mathbf{d}_k \in \mathbb{R}^C\}_{k=1}^K, \quad (9)$$

where K is the variable dictionary length and C is the feature dimension of each dictionary atom.

Each Gaussian primitive i in the scene is assigned a weight vector $\mathbf{w}_i = [w_{i1}, \dots, w_{iK}]^\top$ over the dictionary, so that the semantic feature associated with primitive i is the linear combination

$$\mathbf{f}_i = \sum_{k=1}^K w_{ik} \mathbf{d}_k. \quad (10)$$

We adopted the standard volumetric compositing used in Gaussian splatting. Let the primitives be arranged along a ray. Denote by α_i the opacity (alpha) of primitive i and by T_i the front-surface transmittance up to i :

$$T_i = \prod_{j < i} (1 - \alpha_j). \quad (11)$$

Replacing the usual RGB color \mathbf{c}_i with the semantic feature \mathbf{f}_i , the rendered pixel feature \mathbf{F}_p at pixel (or ray) p is

$$\begin{aligned} \mathbf{F}_p &= \sum_i T_i \alpha_i \mathbf{f}_i = \sum_i T_i \alpha_i \left(\sum_{k=1}^K w_{ik} \mathbf{d}_k \right) \quad (12) \\ &= \sum_{k=1}^K \left(\sum_i T_i \alpha_i w_{ik} \right) \mathbf{d}_k = \sum_{k=1}^K W_k(p) \mathbf{d}_k, \quad (13) \end{aligned}$$

where we define the *rendered weight map* for dictionary atom k as

$$W_k(p) = \sum_i T_i \alpha_i w_{ik}. \quad (14)$$

Equations (12)–(13) show that computing the per-primitive features \mathbf{f}_i and then compositing yields exactly the same result as first compositing scalar weights into per-atom weight maps $W_k(p)$ and then linearly combining dictionary atoms. Because $K \ll C$ and the dictionary atoms \mathbf{d}_k are globally shared, it is far more efficient to (i) render the scalar weight maps $\{W_k(p)\}_{k=1}^K$ and then (ii) form the final feature via a small matrix multiplication

$$\mathbf{F}_p = \mathbf{D}\mathbf{W}(p), \quad (15)$$

where

$$\mathbf{D} = [\mathbf{d}_1, \dots, \mathbf{d}_K] \in \mathbb{R}^{C \times K}, \quad (16)$$

$$\mathbf{W}(p) = [W_1(p), \dots, W_K(p)]^\top \in \mathbb{R}^K. \quad (17)$$

This factorized encoding provides a practical balance between expressiveness and efficiency. The global dictionary captures reusable semantic concepts shared across scenes, whereas the per-primitive weights preserve local variations and spatial specificity. Because the representation separates appearance-independent semantic atoms from their spatial assignments, it can be rendered efficiently while remaining compatible with the Gaussian splatting pipeline.

Algorithm 1 Continuous Semantic Label Collection

Require: Video frames $\{I_t\}_{t=1}^T$, SAMv2, SAM, CLIP

Ensure: Pixel–feature pairs $\{(P_i, F_i)\}_{i=1}^N$

```

1: for each frame  $I_t$  do
2:   Generate candidate masks using SAMv2 and SAM
3:   Apply post-NMS filtering to remove redundant masks
4:   Identify new objects using propagated masks
5:   if first frame or new objects detected then
6:     Propagate masks using SAMv2 predictor
7:   end if
8:   Store object masks  $\{M_{t,k}\}$ 
9: end for
10: for each pixel  $P_i$  in mask  $M_{t,k}$  do
11:    $F_i \leftarrow \text{CLIP}(P_i)$ 
12:   Save  $(P_i, F_i)$ 
13: end for
14: return  $\{(P_i, F_i)\}_{i=1}^N$  on RE10K

```

3.3. Continuous Semantic Label Collection

Our continuous semantic label collection aims to establish 3D semantic paired data by associating each pixel P_i with a rich semantic feature $\mathbf{F}_i \in \mathbb{R}^d$.

As outlined in Alg. 1, we employ SAMv2 [36] and SAM [16] for continuous object-level segmentation. We then use CLIP [34] for semantic extraction. This results in a collection of pixel-feature pairs $\{(P_i, F_i)\}_{i=1}^N$ across the RE10k dataset [57], providing a solid foundation for training. As we obtain segmentation groups, pixels within the n th group share the same gt language feature, which can also be regarded as g_n^{gt} as described in 3.1.

The proposed collection pipeline is intended to reduce the semantic ambiguity commonly found in open-world video data. By combining mask generation, propagation, and post-filtering, we obtain more stable object-level regions over time. These regions provide a consistent basis for extracting continuous semantic features, which are essential for learning dense 3D semantic correspondences.

4. Experiments

We conduct experiments on ScanNet [6] and 3D-OVS [26] to validate the effectiveness of LangFlash. Section 4.1 describes the implementation details of the proposed method. Section 4.2 presents the quantitative results of semantic 3D reconstruction and open-vocabulary segmentation. Section 4.3 provides ablation studies that analyze the impact of each design component.

4.1. Implementation Details

We initialize the geometry prediction layers using NoPoSplat [49], and optimize the entire system end-to-end with

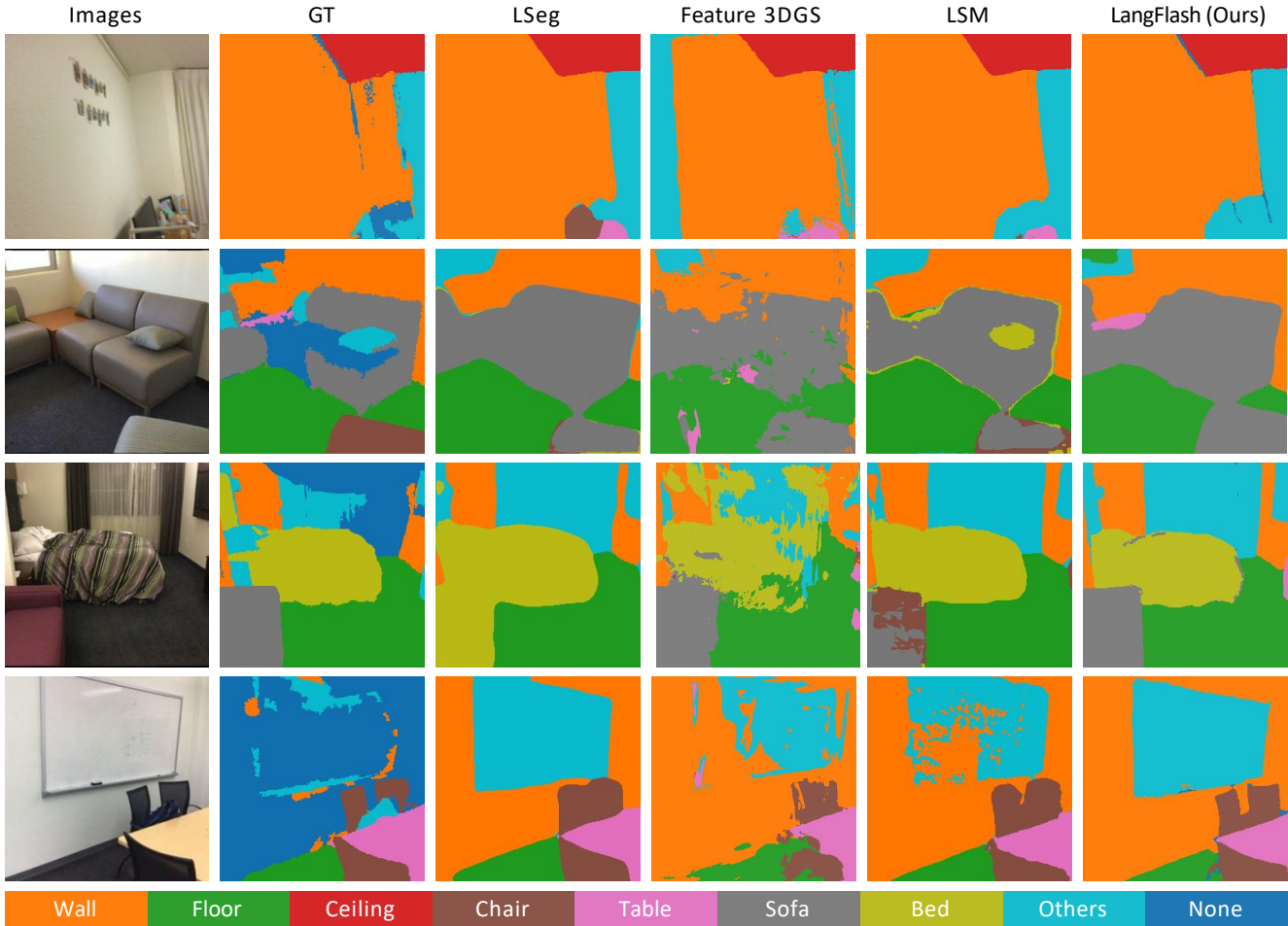


Figure 3. Language-based 3D Segmentation Comparison on ScanNet [6]. We visualize the segmentation results across four unseen scenes and observe that our method performs comparably to previous methods.

Table 1. Quantitative Comparison in 3D Tasks on ScanNet [6]. We report the novel view synthesis and open-vocabulary segmentation accuracy. Our method eliminates the need for any preprocessing in 3D tasks while achieving performance comparable to other baselines that rely on SfM to obtain camera poses.

	Reconstruction Time↓		Source View		Target View (Segmentation)		Target View (Rendering)		
	SfM	Per-Scene	mIoU↑	Acc.↑	mIoU↑	Acc.↑	PSNR↑	SSIM↑	LPIPS↓
LSeg [19]	N/A	N/A	0.5278	0.7654	0.5281	0.7612	-	-	-
NeRF-DFF [17]	20.52s	1min2s	0.4540	0.7173	0.4037	0.6755	19.86	0.6650	0.3629
Feature-3DGS [56]	20.52s	18min36s	0.4453	0.7276	0.4223	0.7174	24.49	0.8132	0.2293
pixelSplat [2]	20.52s	0.064s	-	-	-	-	24.89	0.8392	0.1641
LSM [9]		0.108s	0.5034	0.7740	0.5078	0.7686	24.39	0.8072	0.2506
Ours (zero-shot)		0.180s	0.6217	0.7878	0.6265	0.7861	24.80	0.7906	0.2072
Ours		0.180s	0.7344	0.8746	0.7416	0.8718	24.80	0.7906	0.2072

the loss function described above. For a fair comparison with the LSM [9], we train two versions of the model separately on ScanNet [6] and RE10k [57]. Specifically, the model is trained for 10k steps on ScanNet [6] and 50k steps on RE10k [57]. We use AdamW [29] as the optimizer with

a base learning rate of $2e-4$ for all experiments. For ScanNet [6], evaluation is conducted on 40 unseen scenes, following the same protocol as LSM [9]. In addition to novel-view synthesis, we evaluate the model on 3D language-based semantic segmentation, measuring its ability to align open-

Table 2. Quantitative comparisons of 3D semantic segmentation on the 3D-OVS dataset [26]. We report the mIoU scores (%).

Method	<i>bed</i>	<i>bench</i>	<i>room</i>	<i>sofa</i>	<i>lawn</i>	overall
LSeg [19]	56.0	6.0	19.2	4.5	17.5	20.6
ODISE [47]	52.6	24.1	52.5	48.3	39.8	43.5
FFD [17]	56.6	6.1	25.1	3.7	42.9	26.9
LERF [14]	73.5	53.2	46.6	27	73.7	54.8
Ours (zero shot)	67.8	83.2	64.7	33.3	75.7	64.9

vocabulary queries with consistent 3D representations. For 3D-OVS [26], evaluation is conducted on 5 complex scenes, focusing exclusively on 3D language-based semantic segmentation.

4.2. Semantic 3D Reconstruction

In Table 1, our method achieves the highest accuracy on both the source and target views, demonstrating that the proposed 3D semantic Gaussian field delivers strong open-vocabulary segmentation while maintaining cross-view consistency. Compared with prior 3D approaches, LangFlash shows substantial gains in target-view accuracy, indicating a more discriminative and robust geometry–language representation. Notably, the model trained only on RE10k [57] (“Ours (zero-shot)”), generalizes well to ScanNet [6], confirming strong cross-dataset transfer. Moreover, LangFlash reconstructs each scene in 0.180s without SfM preprocessing, achieving an effective balance between efficiency and accuracy for real-world robotics and embodied AI. The qualitative results (Figures 3 and 4) show semantically coherent structures across views, with consistent boundaries and accurate localization, even in cluttered scenes. The semantic field maintains stable region assignments under large viewpoint changes and preserves object-level continuity in the absence of artifacts. On the 3D-OVS dataset [26] (Table 2), our zero-shot model outperforms both 2D and 3D methods, including LERF [14], demonstrating that LangFlash captures object-level concepts and larger regions reliably. This robustness persists under uneven category distributions and varying lighting and geometries. Failure cases mainly occur for very small or thin objects, reflective surfaces, or fine-grained ambiguous categories but do not affect the overall performance. Overall, LangFlash provides a strong, generalizable, and efficient solution for open-vocabulary 3D semantic segmentation using its 3D-consistent Gaussian representation and robust language–geometry alignment.

4.3. Ablation Studies

We perform ablation experiments to validate the effectiveness of our design choices. All experiments evaluate both

language-driven segmentation and novel-view synthesis, with quantitative segmentation results reported in Table 3. It summarizes the results: PointTransformer-based [44, 45, 54] segmentation (PT, Exp. [1]) is evaluated using ground-truth masks and Hungarian matching; SG with ground-truth masks shows clear improvement (Exp. [2]); SG with averaged LSeg [19] language features yields coarser results (Exp. [3]); and SG with our proposed LFA achieves the best performance (Exp. [4]). These experiments isolate each component under controlled conditions and demonstrate how different design choices affect the overall performance.

Semantic Grouping. We implement a variant of our segmentation module using PointTransformer blocks [44, 45, 54] (denoted as ‘PT’). However, PT relies on highly accurate 3D point coordinates, which are difficult to obtain in a feedforward Gaussian model owing to inherent regression noise. Consequently, the PT-based design is sensitive to small spatial perturbations, which is evident even when evaluated using ground-truth masks. The PT variant shows a clear performance drop compared to our Semantic Grouping (SG) module (Exp. [1] vs. [2] in Table 3), indicating that PT struggles to maintain stable associations under coordinate noise. In contrast, the SG operates reliably in this setting, maintaining a coherent grouping even with imperfect geometry, thereby demonstrating its robustness to geometric variations in feed-forward Gaussian pipelines.

Table 3. Quantitative results of the ablation study for different segmentation implementations and feature aggregation designs.

Exp ID	Model	mIoU↑	Acc.↑
[1]	PT w. gt masks	0.6536	0.8277
[2]	SG w. gt masks	0.7601	0.9214
[3]	SG w. avg feature	0.7273	0.8601
[4]	SG w. LFA	0.7416	0.8718

Language Feature Aggregation. Language–visual models, such as LSeg [19] tend to exhibit local alignment between image and text features. Because of this locality, a naive strategy, such as the simple averaging of per-point language features, can only produce coarse and noisy associations, especially in regions where multiple semantic concepts are spatially intertwined or where language cues vary gradually across the scene. In contrast, our proposed module enables the model to retain finer distinctions while preserving contextual relationships. As shown in Table 3, replacing the LFA with simple averaging (Exp. [3]) leads to a weaker performance. While using our LFA (Exp. [4]) yields noticeably stronger results, reflecting that our aggregation strategy can more effectively emphasize discriminative cues and suppress ambiguous cues.

Dictionary length K . We adopt $K = 128$ as the default

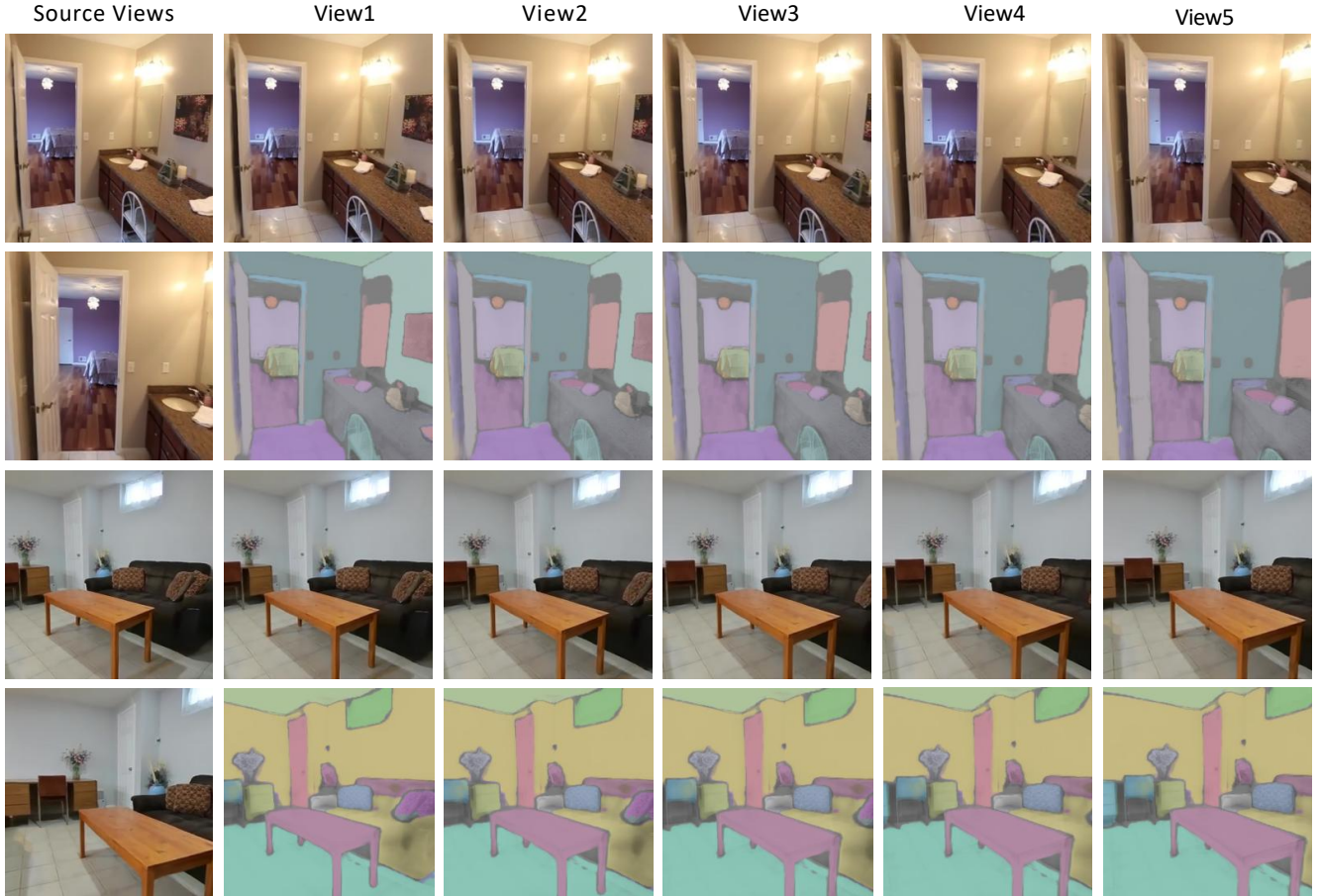


Figure 4. Qualitative results on Re10K. We further visualize both the segmentation and novel-view synthesis results, which demonstrate that our method reconstructs 3D-consistent semantic Gaussian fields with high fidelity.

setting. To analyze the impact of this hyperparameter, we compare different values of K on ScanNet [6] using equal training time. Table 4 validates that our selected value provides a favorable trade-off between performance and speed.

Table 4. Results of Different K on ScanNet

Metric	$K = 64$	$K = 96$	$K = 128$	$K = 196$	$K = 256$
mIoU \uparrow	0.6928	0.6577	0.7144	0.7165	0.7228
Acc. \uparrow	0.7953	0.5131	0.8547	0.8348	0.8439

Runtime analysis. As shown in Table 5, the main computational cost arises from the LFA (72 ms), followed by the SG (38 ms). In contrast, LSeg [19] and the Gaussian decoder are relatively lightweight. The end2end runtime is 180 ms per scene (2 input views), demonstrating its efficiency.

Table 5. Computation Time for Different Components

	LSeg	Shared Encoder	SG	LFA	Gaussian Decoder	All
Time (ms)	6	32	38	72	32	180

5. Conclusion

In this study, we present **LangFlash**, a generalizable and low-latency framework for 3D reconstruction and semantic understanding from sparse views. LangFlash integrates open-vocabulary language features with efficient 3D Gaussian Splatting, predicting geometry, appearance, and semantics in a single forward pass, thereby eliminating the need for per-scene optimization. To support large-scale training and ensure semantic consistency, we enrich the RE10k dataset with temporally coherent semantic annotations and design a novel pipeline comprising *Semantic Grouping* and *Language Feature Aggregation* modules, which extract globally consistent group-wise representations from multi-view RGB images and language features. Our dictionary-based *Sparse Scene Encoding* scheme further compresses the representation, enabling more efficient training while preserving the semantic fidelity and reconstruction accuracy. Experiments show that LangFlash not only supports instant rendering but also delivers substantially improved open-vocabulary semantic reconstruction, demonstrating its strong efficiency and generalization.

Acknowledgements

This work was supported in part by the NIH grant R01HD104969 and the NTU Nanyang Assistant Professorship Startup Grant 025661-00012. This research was also supported in part by Google.org and the Google Cloud Research Credits Program through the Gemma Academic Program.

References

- [1] Nicolas Carion, Francisco Massa, Gabriel Synnaeve, Nicolas Usunier, Alexander Kirillov, and Sergey Zagoruyko. End-to-end object detection with transformers. In *European conference on computer vision*, pages 213–229. Springer, 2020. 3, 4
- [2] David Charatan, Sizhe Lester Li, Andrea Tagliasacchi, and Vincent Sitzmann. pixelsplat: 3d gaussian splats from image pairs for scalable generalizable 3d reconstruction. In *Proceedings of the IEEE/CVF conference on computer vision and pattern recognition*, pages 19457–19467, 2024. 1, 2, 6
- [3] Kangjie Chen, BingQuan Dai, Minghan Qin, Dongbin Zhang, Peihao Li, Yingshuang Zou, and Haoqian Wang. Sl-gaussian: Fast language gaussian splatting in sparse views. In *Proceedings of the 33rd ACM International Conference on Multimedia*, pages 3047–3056, 2025. 2
- [4] Yuedong Chen, Haofei Xu, Chuanxia Zheng, Bohan Zhuang, Marc Pollefeys, Andreas Geiger, Tat-Jen Cham, and Jianfei Cai. Mvsplat: Efficient 3d gaussian splatting from sparse multi-view images. In *European conference on computer vision*, pages 370–386. Springer, 2024. 1, 2
- [5] Bowen Cheng, Alex Schwing, and Alexander Kirillov. Per-pixel classification is not all you need for semantic segmentation. *Advances in neural information processing systems*, 34:17864–17875, 2021. 3
- [6] Angela Dai, Angel X Chang, Manolis Savva, Maciej Halber, Thomas Funkhouser, and Matthias Nießner. Scannet: Richly-annotated 3d reconstructions of indoor scenes. In *Proceedings of the IEEE conference on computer vision and pattern recognition*, pages 5828–5839, 2017. 5, 6, 7, 8
- [7] Jiafei Duan, Samson Yu, Hui Li Tan, Hongyuan Zhu, and Cheston Tan. A survey of embodied ai: From simulators to research tasks. *IEEE Transactions on Emerging Topics in Computational Intelligence*, 6(2):230–244, 2022. 1
- [8] Jixuan Fan, Wanhua Li, Yifei Han, Tianru Dai, and Yansong Tang. Momentum-gs: Momentum gaussian self-distillation for high-quality large scene reconstruction. In *Proceedings of the IEEE/CVF International Conference on Computer Vision*, pages 25250–25260, 2025. 1
- [9] Zhiwen Fan, Jian Zhang, Wenyan Cong, Peihao Wang, Renjie Li, Kairun Wen, Shijie Zhou, Achuta Kadambi, Zhangyang Wang, Danfei Xu, et al. Large spatial model: End-to-end unposed images to semantic 3d. *Advances in neural information processing systems*, 37:40212–40229, 2024. 2, 3, 6
- [10] Jie Hu, Shizun Wang, and Xinchao Wang. Pe3r: Perception-efficient 3d reconstruction. *arXiv preprint arXiv:2503.07507*, 2025. 2
- [11] Lihan Jiang, Yucheng Mao, Linning Xu, Tao Lu, Kerui Ren, Yichen Jin, Xudong Xu, Mulin Yu, Jiangmiao Pang, Feng Zhao, et al. Anysplat: Feed-forward 3d gaussian splatting from unconstrained views. *ACM Transactions on Graphics (TOG)*, 44(6):1–16, 2025. 1, 2
- [12] Lihan Jiang, Yucheng Mao, Linning Xu, Tao Lu, Kerui Ren, Yichen Jin, Xudong Xu, Mulin Yu, Jiangmiao Pang, Feng Zhao, et al. Anysplat: Feed-forward 3d gaussian splatting from unconstrained views. *ACM Transactions on Graphics (TOG)*, 44(6):1–16, 2025. 2
- [13] Bernhard Kerbl, Georgios Kopanas, Thomas Leimkühler, George Drettakis, et al. 3d gaussian splatting for real-time radiance field rendering. *ACM Trans. Graph.*, 42(4):139–1, 2023. 1, 2
- [14] Justin Kerr, Chung Min Kim, Ken Goldberg, Angjoo Kanazawa, and Matthew Tancik. Lurf: Language embedded radiance fields. In *Proceedings of the IEEE/CVF international conference on computer vision*, pages 19729–19739, 2023. 2, 3, 7
- [15] Chung Min Kim, Mingxuan Wu, Justin Kerr, Ken Goldberg, Matthew Tancik, and Angjoo Kanazawa. Garfield: Group anything with radiance fields. In *Proceedings of the IEEE/CVF Conference on Computer Vision and Pattern Recognition*, pages 21530–21539, 2024. 2, 3
- [16] Alexander Kirillov, Eric Mintun, Nikhila Ravi, Hanzi Mao, Chloe Rolland, Laura Gustafson, Tete Xiao, Spencer Whitehead, Alexander C Berg, Wan-Yen Lo, et al. Segment anything. In *Proceedings of the IEEE/CVF international conference on computer vision*, pages 4015–4026, 2023. 4, 5
- [17] Sosuke Kobayashi, Eiichi Matsumoto, and Vincent Sitzmann. Decomposing nerf for editing via feature field distillation. *Advances in neural information processing systems*, 35:23311–23330, 2022. 6, 7
- [18] Vincent Leroy, Yohann Cabon, and Jérôme Revaud. Grounding image matching in 3d with mast3r. In *European conference on computer vision*, pages 71–91. Springer, 2024. 2
- [19] Boyi Li, Kilian Q Weinberger, Serge Belongie, Vladlen Koltun, and René Ranftl. Language-driven semantic segmentation. *arXiv preprint arXiv:2201.03546*, 2022. 1, 3, 4, 6, 7, 8
- [20] Feng Li, Hao Zhang, Huaizhe Xu, Shilong Liu, Lei Zhang, Lionel M Ni, and Heung-Yeung Shum. Mask dino: Towards a unified transformer-based framework for object detection and segmentation. In *Proceedings of the IEEE/CVF conference on computer vision and pattern recognition*, pages 3041–3050, 2023. 3
- [21] Qijing Li, Jingxiang Sun, Liang An, Zhaoqi Su, Hongwen Zhang, and Yebin Liu. Semanticsplat: Feed-forward 3d scene understanding with language-aware gaussian fields. *arXiv preprint arXiv:2506.09565*, 2025. 2
- [22] Wanhua Li, Yujie Zhao, Minghan Qin, Yang Liu, Yuanhao Cai, Chuang Gan, and Hanspeter Pfister. Langsplatv2: High-dimensional 3d language gaussian splatting with 450+ fps. *arXiv preprint arXiv:2507.07136*, 2025. 2
- [23] Wanhua Li, Renping Zhou, Jiawei Zhou, Yingwei Song, Johannes Herter, Minghan Qin, Gao Huang, and Hanspeter Pfister. 4d langsplat: 4d language gaussian splatting via

- multimodal large language models. In *Proceedings of the Computer Vision and Pattern Recognition Conference*, pages 22001–22011, 2025. 2
- [24] Tsung-Yi Lin, Priya Goyal, Ross Girshick, Kaiming He, and Piotr Dollár. Focal loss for dense object detection. In *Proceedings of the IEEE international conference on computer vision*, pages 2980–2988, 2017. 4
- [25] Fangfu Liu, Chubin Zhang, Yu Zheng, and Yueqi Duan. Semantic ray: Learning a generalizable semantic field with cross-reprojection attention. In *Proceedings of the IEEE/CVF Conference on Computer Vision and Pattern Recognition*, pages 17386–17396, 2023. 2, 3
- [26] Kunhao Liu, Fangneng Zhan, Jiahui Zhang, Muyu Xu, Yingchen Yu, Abdulmotaleb El Saddik, Christian Theobalt, Eric Xing, and Shijian Lu. Weakly supervised 3d open-vocabulary segmentation. *Advances in Neural Information Processing Systems*, 36:53433–53456, 2023. 5, 7
- [27] Shilong Liu, Feng Li, Hao Zhang, Xiao Yang, Xianbiao Qi, Hang Su, Jun Zhu, and Lei Zhang. Dab-detr: Dynamic anchor boxes are better queries for detr. *arXiv preprint arXiv:2201.12329*, 2022. 3
- [28] Shilong Liu, Zhaoyang Zeng, Tianhe Ren, Feng Li, Hao Zhang, Jie Yang, Qing Jiang, Chunyuan Li, Jianwei Yang, Hang Su, et al. Grounding dino: Marrying dino with grounded pre-training for open-set object detection. In *European conference on computer vision*, pages 38–55. Springer, 2024. 1
- [29] Ilya Loshchilov and Frank Hutter. Decoupled weight decay regularization. *arXiv preprint arXiv:1711.05101*, 2017. 6
- [30] Zongyang Ma, Guan Luo, Jin Gao, Liang Li, Yuxin Chen, Shaoru Wang, Congxuan Zhang, and Weiming Hu. Open-vocabulary one-stage detection with hierarchical visual-language knowledge distillation. In *Proceedings of the IEEE/CVF conference on computer vision and pattern recognition*, pages 14074–14083, 2022. 1
- [31] Ben Mildenhall, Pratul P Srinivasan, Matthew Tancik, Jonathan T Barron, Ravi Ramamoorthi, and Ren Ng. Nerf: Representing scenes as neural radiance fields for view synthesis. *Communications of the ACM*, 65(1):99–106, 2021. 1, 2
- [32] Fausto Milletari, Nassir Navab, and Seyed-Ahmad Ahmadi. V-net: Fully convolutional neural networks for volumetric medical image segmentation. In *2016 fourth international conference on 3D vision (3DV)*, pages 565–571. Ieee, 2016. 4
- [33] Minghan Qin, Wanhua Li, Jiawei Zhou, Haoqian Wang, and Hanspeter Pfister. Langsplat: 3d language gaussian splatting. In *Proceedings of the IEEE/CVF Conference on Computer Vision and Pattern Recognition*, pages 20051–20060, 2024. 2, 3
- [34] Alec Radford, Jong Wook Kim, Chris Hallacy, Aditya Ramesh, Gabriel Goh, Sandhini Agarwal, Girish Sastry, Amanda Askell, Pamela Mishkin, Jack Clark, et al. Learning transferable visual models from natural language supervision. In *International conference on machine learning*, pages 8748–8763. PmLR, 2021. 5
- [35] René Ranftl, Alexey Bochkovskiy, and Vladlen Koltun. Vision transformers for dense prediction. In *Proceedings of the IEEE/CVF international conference on computer vision*, pages 12179–12188, 2021. 3
- [36] Nikhila Ravi, Valentin Gabeur, Yuan-Ting Hu, Ronghang Hu, Chaitanya Ryali, Tengyu Ma, Haitham Khedr, Roman Rädle, Chloe Rolland, Laura Gustafson, et al. Sam 2: Segment anything in images and videos. *arXiv preprint arXiv:2408.00714*, 2024. 5
- [37] Brandon Smart, Chuanxia Zheng, Iro Laina, and Victor Adrian Prisacariu. Splatt3r: zero-shot gaussian splatting from uncalibrated image pairs (2024). URL <https://arxiv.org/abs/2408.13912>, 2024. 1, 2
- [38] Matthew Tancik, Vincent Casser, Xinchen Yan, Sabeek Pradhan, Ben Mildenhall, Pratul P Srinivasan, Jonathan T Barron, and Henrik Kretzschmar. Block-nerf: Scalable large scene neural view synthesis. In *Proceedings of the IEEE/CVF conference on computer vision and pattern recognition*, pages 8248–8258, 2022. 1
- [39] Ashish Vaswani, Noam Shazeer, Niki Parmar, Jakob Uszkoreit, Llion Jones, Aidan N Gomez, Łukasz Kaiser, and Illia Polosukhin. Attention is all you need. *Advances in neural information processing systems*, 30, 2017. 3
- [40] Jianyuan Wang, Minghao Chen, Nikita Karaev, Andrea Vedaldi, Christian Rupprecht, and David Novotny. Vggt: Visual geometry grounded transformer. In *Proceedings of the Computer Vision and Pattern Recognition Conference*, pages 5294–5306, 2025. 2
- [41] Shuzhe Wang, Vincent Leroy, Yohann Cabon, Boris Chidlovskii, and Jerome Revaud. Dust3r: Geometric 3d vision made easy. In *Proceedings of the IEEE/CVF conference on computer vision and pattern recognition*, pages 20697–20709, 2024. 2
- [42] Yunsong Wang, Tianxin Huang, Hanlin Chen, and Gim Hee Lee. Freesplat: Generalizable 3d gaussian splatting towards free view synthesis of indoor scenes. *Advances in Neural Information Processing Systems*, 37:107326–107349, 2024. 2
- [43] Philippe Weinzaepfel, Thomas Lucas, Vincent Leroy, Yohann Cabon, Vaibhav Arora, Romain Brégier, Gabriela Csurka, Leonid Antsfeld, Boris Chidlovskii, and Jérôme Revaud. Croco v2: Improved cross-view completion pre-training for stereo matching and optical flow. In *Proceedings of the IEEE/CVF International Conference on Computer Vision*, pages 17969–17980, 2023. 3
- [44] Xiaoyang Wu, Yixing Lao, Li Jiang, Xihui Liu, and Hengshuang Zhao. Point transformer v2: Grouped vector attention and partition-based pooling. *Advances in Neural Information Processing Systems*, 35:33330–33342, 2022. 7
- [45] Xiaoyang Wu, Li Jiang, Peng-Shuai Wang, Zhijian Liu, Xihui Liu, Yu Qiao, Wanli Ouyang, Tong He, and Hengshuang Zhao. Point transformer v3: Simpler faster stronger. In *Proceedings of the IEEE/CVF conference on computer vision and pattern recognition*, pages 4840–4851, 2024. 7
- [46] Yanmin Wu, Jiarui Meng, Haijie Li, Chenming Wu, Yahao Shi, Xinhua Cheng, Chen Zhao, Haocheng Feng, Errui Ding, Jingdong Wang, et al. Opegaussian: Towards point-level 3d gaussian-based open vocabulary understanding. *Advances in Neural Information Processing Systems*, 37:19114–19138, 2024. 2, 3

- [47] Jiarui Xu, Sifei Liu, Arash Vahdat, Wonmin Byeon, Xiaolong Wang, and Shalini De Mello. Open-vocabulary panoptic segmentation with text-to-image diffusion models. In *Proceedings of the IEEE/CVF conference on computer vision and pattern recognition*, pages 2955–2966, 2023. [7](#)
- [48] Yifan Xu, Mengdan Zhang, Chaoyou Fu, Peixian Chen, Xiaoshan Yang, Ke Li, and Changsheng Xu. Multi-modal queried object detection in the wild. *Advances in Neural Information Processing Systems*, 36:4452–4469, 2023. [1](#)
- [49] Botao Ye, Sifei Liu, Haofei Xu, Xueting Li, Marc Pollefeys, Ming-Hsuan Yang, and Songyou Peng. No pose, no problem: Surprisingly simple 3d gaussian splats from sparse unposed images. *arXiv preprint arXiv:2410.24207*, 2024. [2](#), [3](#), [5](#)
- [50] Mingqiao Ye, Martin Danelljan, Fisher Yu, and Lei Ke. Gaussian grouping: Segment and edit anything in 3d scenes. In *European conference on computer vision*, pages 162–179. Springer, 2024. [2](#), [3](#)
- [51] Yuhang Zang, Wei Li, Kaiyang Zhou, Chen Huang, and Chen Change Loy. Open-vocabulary detr with conditional matching. In *European conference on computer vision*, pages 106–122. Springer, 2022. [1](#)
- [52] Cheng Zhang, Haofei Xu, Qianyi Wu, Camilo Cruz Gambardella, Dinh Phung, and Jianfei Cai. Pansplat: 4k panorama synthesis with feed-forward gaussian splatting. In *Proceedings of the Computer Vision and Pattern Recognition Conference*, pages 11437–11447, 2025. [1](#), [2](#)
- [53] Hao Zhang, Feng Li, Shilong Liu, Lei Zhang, Hang Su, Jun Zhu, Lionel M Ni, and Heung-Yeung Shum. Dino: Detr with improved denoising anchor boxes for end-to-end object detection. *arXiv preprint arXiv:2203.03605*, 2022. [3](#)
- [54] Hengshuang Zhao, Li Jiang, Jiaya Jia, Philip HS Torr, and Vladlen Koltun. Point transformer. In *Proceedings of the IEEE/CVF international conference on computer vision*, pages 16259–16268, 2021. [7](#)
- [55] Shuaifeng Zhi, Tristan Laidlow, Stefan Leutenegger, and Andrew J Davison. In-place scene labelling and understanding with implicit scene representation. In *Proceedings of the IEEE/CVF International Conference on Computer Vision*, pages 15838–15847, 2021. [2](#), [3](#)
- [56] Shijie Zhou, Haoran Chang, Sicheng Jiang, Zhiwen Fan, Zehao Zhu, Dejia Xu, Pradyumna Chari, Suyu You, Zhangyang Wang, and Achuta Kadambi. Feature 3dgs: Supercharging 3d gaussian splatting to enable distilled feature fields. In *Proceedings of the IEEE/CVF Conference on Computer Vision and Pattern Recognition*, pages 21676–21685, 2024. [2](#), [3](#), [6](#)
- [57] Tinghui Zhou, Richard Tucker, John Flynn, Graham Fyffe, and Noah Snavely. Stereo magnification: Learning view synthesis using multiplane images. *arXiv preprint arXiv:1805.09817*, 2018. [2](#), [5](#), [6](#), [7](#)
- [58] Siting Zhu, Guangming Wang, Xin Kong, Dezhi Kong, and Hesheng Wang. 3d gaussian splatting in robotics: A survey. *arXiv preprint arXiv:2410.12262*, 2024. [1](#)

LangFlash: Feed-forward 3D Language Gaussian Splatting from Sparse Unposed Images

Supplementary Material

Table 6. Statistics of the processed RE10k dataset.

Metric	Value
Total frames	~6M
Number of scenes	~10k
Avg. masks per image	36
Avg. mask coverage per image (%)	83.5
Processing time (single NVIDIA A100)	30 days

6. RE10k Qualitative visualizations

The visual results shown in Fig. 5 provide a qualitative overview of our performance on the RE10k dataset. These examples were selected to emphasize the characteristic challenges in the dataset: numerous small and overlapping object instances, wide lighting variation, and strong view-point changes that stress both 2D segmentation and multi-view rendering. These qualitative results complement the numerical summary.

7. RE10k Dataset statistics

The table above (Tab. 6) summarizes the primary corpus-level statistics of the processed RE10k split used in this study. In total, we retained approximately six million frames across roughly ten thousand scenes; on average, each image contained dozens of instance masks, with mask pixels covering the majority of the image area. The reported processing time corresponds to running the full pipeline (mask extraction, per-frame cleanup, and multi-view consolidation) on a single NVIDIA A100; in practice, the pipeline is embarrassingly parallel, and the wall-clock time can be reduced by distributed execution.

8. RE10k 3D semantic segmentation

In addition to 4, we annotated five previously unseen scenes and report the per-scene mIoU as well as the average overall score in Tab. 7. The baseline methods (LSeg and LSM) struggled on several scenes, whereas our method achieved substantially higher per-scene and overall mIoU, indicating more consistent cross-view semantic aggregation. These results validate both the quality of the processed dataset and the effectiveness of our proposed approach for 3D semantic segmentation of large-scale, real-world indoor footage.



Figure 5. Additional qualitative results on RE10k. We visualize both the semantic and novel-view synthesis results.

Table 7. 3D semantic segmentation on RE10k (mIoU, %). We assign scene names (absent in the original dataset) and provide their corresponding original identifiers.

Method	<i>Bedroom(5aca)</i>	<i>Aisle(bc95)</i>	<i>Living room (6558)</i>	<i>Study room(89ea)</i>	<i>Pool(cd74)</i>	Overall
LSeg	29.60	18.64	19.12	45.84	14.48	25.53
LSM	24.39	11.67	23.33	42.95	24.77	25.42
Ours	34.33	22.37	34.97	57.44	37.99	37.42